JAAS

ROYAL SOCIETY OF CHEMISTRY

PAPER

View Article Online
View Journal | View Issue

Cite this: *J. Anal. At. Spectrom.*, 2025, **40**, 1964

Capabilities and limitations of Se isotopic analysis using hydride generation coupled to MC-ICP-MS†

Lana Abou-Zeid, *[a] Martin Wiech [b] and Frank Vanhaecke [a]

This study presents a comprehensive methodological investigation aimed at optimizing selenium (Se) isotopic analysis using MC-ICP-MS. Fundamental aspects of the plasma were revisited through spatial profiling, enabling detailed characterization of the distribution of Se^+ and $ArAr^+/ArArH^+$ species within the plasma. Increasing the sampling depth (sampling further upstream in the plasma) proved more effective than the commonly employed methane addition, offering a more effective suppression of the Ar-based species, although at the cost of some loss in the sensitivity for Se. Under these conditions, precision values (expressed as 2SD) of 0.03‰ and 0.17‰ were obtained for $\delta^{82/78}$Se and of 0.08‰ and 0.38‰ for $\delta^{82/76}$Se, at 100 and 25 μg L^{-1}, respectively. Moreover, the method proved robust, with a long-term reproducibility of 0.07‰ (2SD, $n = 120$) and high accuracy, even at up to 30% sample-standard concentration mismatch. However, the method's relatively high hydride formation rate ($\sim 7 \times 10^{-3}$) limits its applicability to samples with As/Se post-isolation ratios ≤0.05, beyond which mathematical corrections lead to biased results. Finally, the method was validated using the SELM-1 reference material, for which the $\delta^{82/78}$Se and $\delta^{82/76}$Se values were in excellent agreement with published data, and was subsequently applied to a set of tuna fish organs (liver, spleen, kidney, and intestine). This study demonstrates that the method that was developed, optimized and validated forms a solid basis for further investigating Se metabolic pathways in marine fish and for elucidating its role in Hg detoxification.

Received 17th May 2025
Accepted 23rd June 2025

DOI: 10.1039/d5ja00196j

rsc.li/jaas

1. Introduction

Selenium (Se) is an essential trace element for living organisms and plays a key role in environmental systems as it is involved in several bio(geo)chemical processes. In the human body, Se is mainly incorporated into proteins and enzymes such as glutathione peroxidases (GPxs) and thioredoxin reductases (TrxRs), mainly involved in antioxidant defense and redox state regulation.[1,2] Studies have shown that insufficient Se levels are associated with diseases such as cancer, diabetes, and immune disorders,[2] further highlighting the importance of Se in human health. Moreover, Se plays a critical protective role against mercury (Hg) toxicity in both humans and animals[3] by forming biologically inert HgSe nanoparticles, as evidenced in marine mammals[4–6] and seabirds,[7] making Se of great interest in marine ecotoxicology and food safety. Despite its essential role, Se can become toxic at concentrations just 3- to 5-fold above the optimal intake, and this duality defined Se as the "double-edged sword element".[8]

Selenium has six stable isotopes with masses ranging from 74 to 82 amu and occurs in multiple redox states, *i.e.* Se(0), Se(−II), Se(IV) and Se(VI), which are involved in several environmental and biogeochemical processes.[9–11] Due to their mass difference, Se isotopes participate with slight differences in the reaction rate (kinetically governed isotope fractionation) and/or in the equilibrium state (thermodynamically governed isotope fractionation) in chemical reactions, leading to isotopic fractionation.[12] This makes Se isotopic analysis highly valuable for tracing Se sources in the environment and understanding its redox cycling and metabolic transformations in natural systems.[13–16] Selenium isotopic analysis is typically performed using multi-collector inductively coupled plasma-mass spectrometry (MC-ICP-MS) due to the high sample throughput and high precision typically offered by this technique.[17,18] However, MC-ICP-MS isotopic analysis of Se is associated with numerous challenges. First, Se has a high ionization potential (9.75 eV), resulting in a relatively poor ionization yield in the ICP source (30%)[19] and therefore, a lower sensitivity compared to other elements. This poses the first challenge for precise isotope ratio measurements, as a reduced ion beam intensity can lead to higher uncertainty (counting statistics), while in most sample types, Se is present at very low concentrations only. To mitigate this lower sensitivity, Se is commonly introduced into the MC-ICP-MS unit under "dry plasma conditions" using a hydride

[a]*Atomic & Mass Spectrometry – A&MS Research Unit, Department of Chemistry, Ghent University, Campus Sterre, Krijgslaan 281 – S12, 9000 Ghent, Belgium. E-mail: lana.abouzeid@ugent.be*

[b]*Institute of Marine Research, PO Box 1870, Nordnes, 5817 Bergen, Norway*

† Electronic supplementary information (ESI) available. See DOI: https://doi.org/10.1039/d5ja00196j

generation (HG) system.[20–23] The latter involves the reduction of Se(IV) by sodium borohydride ($NaBH_4$), resulting in the formation of gaseous Se-hydride. This introduction system increases the Se introduction efficiency in comparison to the standard wet plasma approach using a pneumatic nebulizer and spray chamber and therefore results in an enhanced Se signal intensity. Unfortunately, HG is not Se-selective and other hydride-forming elements such as Ge and As are also converted into gaseous hydrides by $NaBH_4$ and further introduced into the MC-ICP-MS unit, causing spectral interferences affecting the signals of the Se isotopes (overlap of the signals of $^{74}Ge^+$ and $^{74}Se^+$, $^{75}AsH^+$ and $^{76}Ge^+$ and $^{76}Se^+$, and $^{76}GeH^+$ and $^{77}Se^+$). Moreover, the HG process is susceptible to interferences from transition metal ions from elements such as cobalt (Co), copper (Cu), nickel (Ni), and iron (Fe) if present in the sample. These elements are reported to inhibit the conversion of Se(IV) into Se-hydride form, leading to a reduction in Se ion signal intensity.[24] Therefore, a chemical purification prior to HG-MC-ICP-MS measurement is necessary to separate Se from these interfering elements. This is typically accomplished using the well-established thiol cellulose powder (TCP) method, as it ensures quantitative Se recovery and provides optimal separation efficiency from these interfering elements.[24] However, any Se loss during chromatographic isolation may induce isotopic fractionation, thereby compromising the accuracy of isotope ratio measurements. To address this limitation, the double-spike approach is often used, which involves adding a known mixture of enriched Se isotopes to the sample, allowing one to correct for these losses and for instrumental mass discrimination occurring at the level of the MC-ICP-MS. Despite the advantages offered by this approach, it is costly, labor-intensive and requires meticulous sample preparation, while the analysis of samples with an isotopic composition that deviates substantially from the natural one can require longer rinsing to avoid cross-over contamination due to memory effects.

Another significant challenge in Se isotope ratio measurement using MC-ICP-MS is the occurrence of spectral interferences, primarily arising from argon-based polyatomic ions, the signals of which overlap with those of most of the Se isotopes. The most important ones are argon (Ar) dimers, formed by the combination of different Ar isotopes, *i.e.* $^{40}Ar^{36}Ar^+$ and $^{38}Ar^{38}Ar^+$ (both to a lesser extent), $^{40}Ar^{38}Ar^+$ and especially $^{40}Ar^{40}Ar^+$, the signals of which overlap with those of ^{76}Se, ^{78}Se and ^{80}Se, respectively, in addition to $^{40}Ar^{37}Cl^+$, which interferes with the monitoring of ^{77}Se. These interferences are impossible to resolve using a "traditional" MC-ICP-MS not equipped with a collision/reaction cell, as the mass resolution required exceeds the capabilities of the commercially available instrumentation.[17] One of the most effective strategies reported to mitigate this problem is the introduction of methane gas (CH_4) into the plasma,[25,26] which has been adopted by many researchers for Se isotope ratio measurement and is typically accomplished by introducing CH_4 through the hydride generation unit.[21,22,27] Already an amount as low as 1–3 mL min^{-1} of 2% CH_4 in Ar was shown to successfully decrease the signal intensity of $ArAr^+$ and $ArArH^+$ ions by nearly a factor of 2 and at the same time increase the Se signal intensity by approximately a factor of 1.5, resulting in an improved Se/interference ratio, and therefore, in more accurate Se isotope ratio measurements.[26] However, while this solution significantly reduced the formation of Ar-based interferences, it did not eliminate them entirely, further restricting accurate Se isotope ratio measurements at low concentration levels.

Using an MC-ICP-MS equipped with a collision/reaction cell (CRC) nowadays is probably the most effective solution for eliminating Ar-based interferences affecting the Se^+ signals. However, this type of instrumentation was introduced relatively recently only, such that the large majority of all MC-ICP-MS instrumentation used worldwide is not equipped with a CRC. Moreover, the MC-ICP-MS units equipped with a CRC are also substantially more expensive. Therefore, in this work, we present an alternative approach for reducing the spectral overlap of the Ar-based interferences hampering Se isotopic analysis through revisiting some fundamental aspects of the plasma using a "traditional" MC-ICP-MS unit. For this aim, radial and axial profiling of the plasma was conducted in order to elucidate the distribution of $ArAr^+$, $ArArH^+$ and Se^+ ions. These profiles enabled the selection of an optimal torch position such that plasma regions with reduced formation of the interfering ions are extracted *via* the sampling cone orifice, thereby enhancing the Se/interference signal ratio. In addition, the effect of the torch position on the accuracy and precision of Se isotope ratio data was also evaluated. The results obtained under these optimized instrument settings were compared to those achieved using the widely adopted CH_4 addition approach. Moreover, TCP was used for separating Se from matrix elements, ensuring quantitative Se recovery, thereby eliminating the requirement for a double-spike approach. Finally, the method was validated using the selenium-enriched yeast (SELM-1) reference material, previously characterized for its Se isotopic composition by several groups and was applied to a set of tuna fish organs as a proof-of-concept application. This method paves the way to more routine studies of the Se isotopic signature as an additional source of information for revealing the metabolic pathways of Se in fish and further elucidating its role in Hg detoxification.

2. Experimental part

2.1. Chemicals

Sodium borohydride ($NaBH_4$), sodium hydroxide (NaOH), Sigmacell cellulose (type 20, particle size 20 μm), thioglycolic acid (98%), acetic anhydride ReagentPlus® ≥99%, glacial acetic acid ReagentPlus® ≥99% and hydrogen peroxide H_2O_2 9.8 M were purchased from Sigma-Aldrich (Belgium). Sulfuric acid 95–98% Primer Plus™ for trace metal analysis was purchased from Fisher scientific (France). HCl and HNO_3 were supplied by Fisher Chemicals (UK) and further subjected to sub-boiling distillation in a Savillex DST purification system (Savillex, USA). Ultrapure water (18.2 MΩ cm at 25 °C, further referred to as MQ) was obtained from a Milli-Q purification system from Millipore (France). The NIST SRM 3149 Se standard was supplied by the National Institute of Standards and Technology (NIST, USA), Se standard solution (Lot Number HC44697996) was purchased from MERCK (Belgium). The Selenium-enriched

yeast certified reference material (SELM-1) was purchased from the National Research Council Canada (NRC).

2.2. Samples

Atlantic bluefin tuna (ABFT) *Thunnus thynnus* were caught by recreational fishers with a rod and line in summer and autumn along the Norwegian coast. In this work, organ samples from one individual were analysed as a proof-of-principle application. The tuna was caught on August 21st 2020, measured 244 cm (standard fork length) and had an estimated age of 15.8 ± 2.4 years.[6] The samples were obtained fresh on site when the fish was landed with clean sampling devices, and stored frozen in clean, sterile, plastic bags until analysis. All samples were homogenized before and after freeze-drying.

2.3. Sample preparation

All sample preparation was carried out in a class-10 clean lab (PicoTrace, Germany).

2.3.1. Sample digestion. Certified reference materials and samples were taken into solution *via* microwave-assisted acid digestion using a Multiwave 7000 unit (Anton Paar, Belgium). Depending on the Se concentration, approximately 0.1–1 g of material was weighed into a pre-cleaned TFM (modified polytetrafluoroethylene PTFE) microwave vessel. Digestion was carried out using 4 mL of 14 M HNO_3 and 1 mL of 9.8 M H_2O_2 using the following microwave program: 0–20 min: ramp up to 220 °C at 140 bar, 20–30 min: 220 °C at 140 bar, 30–50 min: cooling down. The digest thus obtained was subsequently transferred using 2 mL MQ water into a pre-cleaned PFA (perfluoroalkoxy) beaker and further subjected to evaporation to near dryness at 60 °C. After evaporation, the sample was taken up in 6 M HCl. The beaker was subsequently closed and left on a hotplate at 110 °C for 4 hours to fully reduce Se(VI) to Se(IV).

2.3.2. Sample purification using thiol cellulose powder (TCP). TCP was synthesized according to the method described by Elwaer *et al.* in 2008.[24] 0.1 g of the synthetized TCP (0.5 mL of wet TCP) was loaded into a BioRad column with an internal diameter of 0.8 cm (Eichrom Technologies, France). The resin was washed with 2 mL MQ, followed by 2 mL of 6 M HCl, and then conditioned using 2 mL of 1 M HCl. Finally, 2 mL of sample solution in 1 M HCl was loaded onto the column. The flow rate was accelerated and controlled using a polycarbonate vacuum box (Triskem, France) and was set at approximately 7 mL min^{-1}. The matrix was washed off with 2 mL MQ, 2 mL of 6 M HCl and 2 mL of 1 M HCl. Finally, the resin was left to dry, transferred from the column into a falcon tube and 500 μL of MQ and 500 μL of 14 M HNO_3 were added. Se was extracted from TCP by heating the falcon tubes in a water bath at 95 °C for 20 min. After completing the extraction, 2 mL of MQ water was added into the falcon tube, and the latter was centrifuged at 4 rpm for 5 min. The extraction procedure was repeated once more to ensure a complete extraction of Se from the TCP. The first and the second extract were mixed (total volume $V = 6$ mL), and transferred into a pre-cleaned PFA beaker from which the solvent was evaporated at 60 °C. The residue was collected with 6 M HCl, subjected to a reduction step at 110 °C to ensure complete reduction of Se(VI) to Se(IV) and finally diluted to 100 μg L^{-1} in 2 M HCl for isotope ratio measurements using HG-MC-ICP-MS.

2.4. Instrumentation

2.4.1. Multi-collector inductively coupled plasma-mass spectrometry (MC-ICP-MS). Selenium was introduced into a Neptune XT MC-ICP-MS unit (Thermo Scientific, Germany) in the form of gaseous Se-hydride (H_2Se) using a CETAC HGX 200 hydride generator unit (Teledyne CETAC Technologies, USA). The generation of Se-hydride is based on the reaction of Se(IV) with $NaBH_4$ following eqn (1):

$$3NaBH_4 + 3H_2O + 3HCl + 2H_2SeO_3 \rightarrow 3NaCl + 2H_2Se + 3H_3BO_3 + 6H_2 \quad (1)$$

In the hydride generation (HG) unit, the sample is first acidified with 2 M HCl solution in a mixing tee (Mixing Tee 1 in Fig. S1†). Subsequently, it is mixed with $NaBH_4$ (0.4% w/v in 0.1 M NaOH) in a second mixing tee (Mixing Tee 2), and is allowed to react with $NaBH_4$ in a mixing loop, resulting in the reduction of Se(IV) to Se(−II), in the form of H_2Se.

Selenium is then introduced into the MC-ICP-MS unit under dry conditions. For the experiments involving CH_4 addition, a CH_4/Ar (2/98 mol%) gas mixture (Air liquid, Belgium) was introduced in the additional gas port (Fig. S1†).

The instrument settings of the HG unit and MC-ICP-MS instrument are summarized in Table 1.

The signal intensity was monitored at all m/z using Faraday cups connected to amplifiers equipped with 10^{11} Ω resistors, except at $m/z = 80$, at which the signal intensity was monitored using a Faraday cup connected to an amplifier equipped with a 10^{10} Ω resistor, which can tolerate higher currents without saturation.

Se isotope ratios were reported in the delta notation, as per mil deviation (‰), relative to the NIST SRM-3149 standard:

$$\delta^{82/x}\mathrm{Se}(‰) = \left(\frac{\left(\frac{^{82}\mathrm{Se}}{^{x}\mathrm{Se}}\right)_{\mathrm{sample}}}{\left(\frac{^{82}\mathrm{Se}}{^{x}\mathrm{Se}}\right)_{\mathrm{NIST\ SRM\ 3149}}} - 1 \right) \times 1000 \quad (2)$$

with x being 76 or 78.

The bias induced by instrumental mass discrimination was corrected for using the sample-standard bracketing approach (SSB), by measuring the NIST SRM 3149 standard before and after each sample. Interference correction will be further detailed in Section 2.4.

2.4.2. Inductively coupled plasma-tandem mass spectrometry (ICP-MS/MS). An 8800 Agilent inductively coupled plasma-tandem mass spectrometry ICP-MS/MS unit (Agilent Technologies, Japan) equipped with a MicroMist nebulizer, a Peltier cooled spray chamber, a 2 mm internal diameter injector and nickel cones was relied upon for Se quantification. Se was monitored in mass shift mode, using O_2 as a reaction gas in the collision/reaction cell (CRC). Se levels were quantified by means of external calibration using Te as an internal standard

Table 1 Operating parameters of the HG unit and MC-ICP-MS instrument for Se isotope ratio measurements

Hydride generation unit									
Solution			Composition					Uptake rate	
HCl			2 M					0.182 mL min^{-1}	
$NaBH_4$			0.4% w/v in 0.1 M NaOH					0.182 mL min^{-1}	
Sample			2 M HCl					0.364 mL min^{-1}	
MC-ICP-MS cup configuration									
Cup	L4	L3	L2	L1	C	H1	H2	H3	H4
Mass	73	75	76	77	78	80	81	82	83

MC-ICP-MS			
Instrument settings		Data acquisition parameters	
Sampling cone	Ni; Jet-type; 1.1 mm Ø orifice	Integration time	4.194 s
Skimmer	Ni; X-type; 0.8 mm Ø orifice	Uptake time	240 s
Plasma gas flow rate	15 L min^{-1}	Measurement	1 block, 60 cycles
Auxiliary gas flow rate	0.7 L min^{-1}	Mass resolution	Low
Carrier gas flow rate (HG)	1.2 L min^{-1}		
Additional gas flow rate (HG)	0 L min^{-1}		
RF power (W)	1200		

(IS) to correct for potential matrix effects and signal instability. Additionally, also the potential presence of the interfering elements Fe, Co, Ni, Cu, and As was monitored. These elements were determined in mass-shift mode, with NH_3 introduced into the CRC for Fe, Co, Ni, and Cu, and O_2 for As. Quantification was carried out using external calibration with Ga as an internal standard. The ICP-MS/MS instrument settings and the ion products monitored are summarized in Table 2.

2.5. Interference correction for Se signals in MC-ICP-MS measurements

Several corrections were applied to correct the signals obtained for the Se isotopes for contributions from the $ArAr^+$ ions, hydride ions ($ArArH^+$, BrH^+, and SeH^+) and traces of As potentially present after TCP purification. These corrections are described below. As the Ge concentration detected in the targeted fish samples was lower than the limit of detection, Ge was not considered as a potential interferent and therefore, no Ge correction was developed or performed.

Table 2 ICP-MS/MS instrument settings and data acquisition parameters used for Se quantification

Plasma conditions	
Plasma gas flow rate (L min^{-1})	15
Auxiliary gas flow rate (L min^{-1})	0.9
RF power (W)	1550
Nebulizer gas flow rate (L min^{-1})	1.0
Optional gas	NA
Reaction gas flow rate – O_2 (mL min^{-1})	0.45 (30%)
Ions monitored	$^{80}Se^{16}O^+$, $Co(NH_3)_2^+$, $Ni(NH_3)_2^+$, $Fe(NH_3)_2^+$, $Cu(NH_3)_2^+$, AsO^+, Te^+ (IS) and Ga^+ (IS)
Integration time (s)	1
Replicates	10
Sweeps	100

2.5.1. Evaluation of correction for the occurrence of $ArAr^+$. To correct for Ar-based interferences, an on peak zero (OPZ) or blank subtraction is performed. For this purpose, a 2 M HCl blank sample was measured before and after each sample/standard. The average signal of the two blanks was then subtracted from the signal at the m/z values of 76, 78 and 82. For an accurate OPZ correction, the 2 M HCl blank used for the correction was derived from the same acid batch used to prepare the samples and the standards. In addition to Ar-based interferences, OPZ subtraction also allows to correct for potential trace impurities of Kr in Ar, which leads to isobaric interferences affecting ^{78}Se, ^{80}Se and ^{82}Se, and to correct for $^{81}BrH^+$ (Br contamination in HCl) which interferes with the monitoring of ^{82}Se.

For obtaining the net signal for ^{80}Se, the following calculations were performed:

After correcting for the ^{82}Kr interference by means of OPZ subtraction, $^{82}Se_{(corr)}$ can be used to calculate the signal of ^{80}Se using the natural abundances of the Se isotopes (eqn (3)).

$$^{80}Se_{calc}{}^{+} = I^{82}Se_{(corr)}{}^{+} \times \frac{\text{nat.ab}_{^{80}Se}}{\text{nat.ab}_{^{82}Se}} \quad (3)$$

with nat.ab = natural abundance and I = signal intensity.

Subsequently, the signal for $^{40}Ar^{40}Ar^+$ can be calculated using eqn (4).

$$^{40}Ar^{40}Ar_{(calc)}{}^{+} = I(80) - {}^{80}Se_{calc}{}^{+} \quad (4)$$

Using the natural abundances of the Ar isotopes, the contribution from $ArAr^+$ ions at $m/z = 76$ and 78 can be calculated as described in eqn (5) and (6).

$$^{76}ArAr_{(calc)}{}^{+} = {}^{40}Ar^{40}Ar_{(calc)}{}^{+} \times \frac{\left(\text{nat.ab}_{^{36}Ar^{40}Ar} + \text{nat.ab}_{^{38}Ar^{38}Ar}\right)}{\left(\text{nat.ab}_{^{40}Ar^{40}Ar}\right)} \quad (5)$$

$$^{78}ArAr_{(calc)}{}^{+} = {}^{40}Ar^{40}Ar(calc)^{+} \times \frac{\left(\text{nat.ab}_{^{38}Ar^{40}}\right)}{\left(\text{nat.ab}_{^{40}Ar^{40}Ar}\right)} \quad (6)$$

These calculated $ArAr^+$ signals were only used to evaluate the contribution from these interferences to the signals at $m/z = 76$ and 78. The contribution (%) was calculated by dividing the calculated signal intensity for $^{76}ArAr_{(calc)}{}^{+}$ and $^{78}ArAr_{(calc)}{}^{+}$ by the total signal intensity at mass 76 and 78, respectively. As the occurrence of $ArAr^+$ ions was minimized to the maximum extent (see the Results and discussion section), an OPZ subtraction was sufficient to correct for this contribution. The additional correction using these estimated signals only added errors to the final results.

2.5.2. Evaluation of correction for the occurrence of hydride ions. Se tends to form SeH^+ hydride ions which overlap with the signals of the Se^+ atomic ions at mass $M + 1$. For instance, the signals of $^{77}SeH^+$ and $^{78}Se^+$ overlap. In addition, As, potentially present as traces in the Se fraction after TCP purification, can also form a hydride ion ($^{75}AsH^+$), which interferes with the measurement of ^{76}Se. To correct for these interferences, the hydride generation rate was calculated as shown in eqn (7):

$$\text{HG rate} = \frac{I(83)_{corr}}{I(82)_{corr}} = \frac{^{82}SeH}{^{82}Se_{corr}} \quad (7)$$

with $I(83)_{corr}$, the intensity at $m/z = 83$ corrected for the contribution from ^{83}Kr using the OPZ subtraction.

The HG rate is typically very stable throughout a measurement session and is assumed to be the same for all Se isotopes. Therefore, the HG rate was used to correct the signal obtained at $m/z = 78$ for the contribution from $^{77}SeH^+$ as shown in eqn (8) and (9):

$$^{77}SeH^+ = {}^{77}Se^+ \times \text{HG rate} \quad (8)$$

$$^{78}Se_{corr}{}^{+} = I(78) - {}^{77}SeH^+ \quad (9)$$

with $I(78)$ corrected for the $ArAr^+$ interferences using the OPZ subtraction.

In the case of As, it is assumed that the AsH^+/As^+ ratio is identical to $^{82}SeH^+/^{82}Se^+$. Therefore, the HG rate was also used to correct the signal at $m/z = 76$ for the contribution from $^{75}AsH^+$ as shown in eqn (10) and (11):

$$^{75}AsH^+ = {}^{75}As_{corr}{}^{+} \times \text{HG rate} \quad (10)$$

$$^{76}Se_{corr}{}^{+} = I(76) - {}^{75}AsH^+ \quad (11)$$

with $^{75}As_{corr}{}^{+}$, the signal at $m/z = 75$ corrected for the $^{40}Ar^{35}Cl^+$ contribution using the OPZ subtraction.

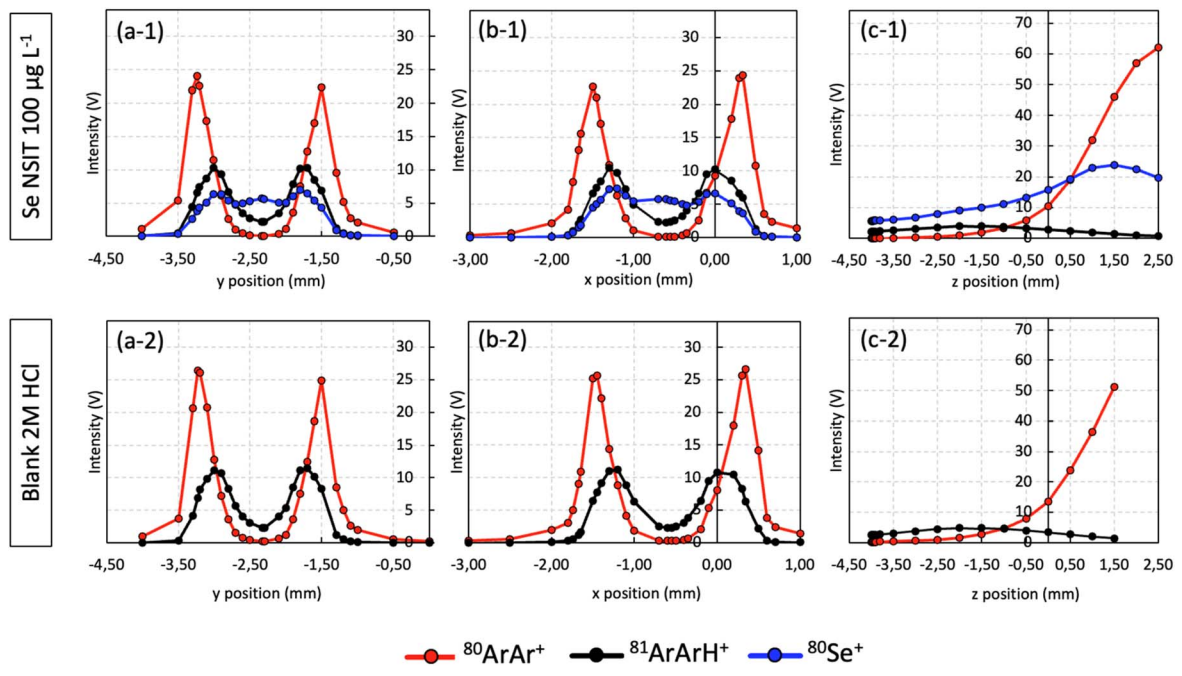

Fig. 1 Radial (x, y) and axial (z) spatial profiling of $^{80}ArAr^+$, $^{81}ArArH^+$ and $^{80}Se^+$ with a fixed carrier gas flow rate of 1.2 L min^{-1}. For radial profiling, the z position was fixed at −4.0 mm.

3. Results and discussion

3.1. Effect of plasma parameters on Ar-based interferences

It is well established that the ion beam analyzed by the mass spectrometer does not originate from a single point in the plasma, but from a cylindrical volume of plasma with a diameter of *ca.* 0.25 mm and a depth of *ca.* 2 mm (sample volume of *ca.* 0.14 mm^3) in front of the sampling cone aperture.[28] To investigate the distribution of Se^+ ions and of interfering species, particularly $ArAr^+$ and $ArArH^+$, within the plasma, axial and radial spatial profiling were performed. For this aim, a 100 $\mu g\ L^{-1}$ Se NIST elemental solution was introduced into the MC-ICP-MS unit *via* the HG unit and the signals at $m/z = 81$ (corresponding to $ArArH^+$) and 80 (which includes contributions from both $^{80}Se^+$ and $^{80}ArAr^+$, calculated according to eqn (3) and (4)) were recorded at various x, y, and z torch positions (Fig. 1(a-1) to (c-1)). The same experiment was conducted using a blank solution of 2 M HCl (Fig. 1(a-2) to (c-2)) for monitoring the signal of the interfering ions in the absence of Se.

As can be seen in Fig. 1, the profiles obtained with and without Se in solution are nearly identical, with Ar-based interference intensities remaining consistent, even when experiments were conducted on different days. This observation aligns with the findings of Pogge von Strandmann *et al.*,[29] who used HG coupled to a sector field ICP-MS unit operated in high resolution mode to monitor the stability of Ar-based interfering signals. The authors showed that the intensity obtained for $ArAr^+$ was identical with and without Se present in solution, and stable throughout the measurement session.[29]

Furthermore, as shown in Fig. 1(a-1) and (b-1), the radial profiles of $ArAr^+$ and $ArArH^+$ exhibit a distinct double or bimodal peak shape, in accordance with the observations of Fraser and Beauchemin.[30] The profiles reveal two maxima at distinct positions: −3.23 mm and −1.5 mm on the y-axis, and −1.5 mm and 0.3 mm on the x-axis, with maximum signal intensities of approximately 25 V for $^{80}ArAr^+$ and 10 V for $ArArH^+$. At the central position between the two peaks (2.33 mm on the y-axis and −0.6 mm on the x-axis), a minimum intensity is observed for the interfering species with 0.05 V for $^{80}ArAr^+$ and 2.22 V for $ArArH^+$, being respectively 500- and 4.5-fold lower than those observed at the maxima of each peak. Moreover, a maximum contribution from the $^{80}Se^+$ signal at $m/z = 80$ is observed at this position with an intensity of 5.70 V, making these x and y values optimal for a high Se/interference ratio. Following this observation, the y and x positions were fixed at −0.6 mm and 2.33 mm, respectively, and the z position of the torch (sampling depth or distance between the tip of the torch and the sampling cone aperture) was changed from 2.5 mm (torch at the furthest position from the sampler cone, thus sampling further downstream in the ICP), to 0 mm as the central position (medium position), and finally to −4 mm (torch at the closest position to the sampler cone, thus sampling more upstream in the ICP), as reported in Fig. 1(c-1) and (c-2). The axial profile reveals a different behavior of the Se^+ and interfering ion species, respectively. For $^{80}ArAr^+$, the signal exhibits a maximum of 62 V at 2.5 mm and decreases when bringing the torch closer to the sampling cone, reaching 0.27 V at −4 mm. For $^{80}Se^+$, the signal displays a slight increase first, reaching a maximum of 23.83 V at 1.5 mm, before slowly decreasing to 5.47 V at −4 mm. This observation is in accordance with previous observations from Holliday and Beauchemin who stated that sampling more upstream in the plasma results in reduced signal intensity due to the short residence time of the analyte in the plasma.[28] Finally, for $ArArH^+$, an increase is first observed, reaching a maximum of 4.82 V at −2 mm after which the signal decreases to a minimum of 2.48 V at −4 mm. Based on these results, it can be concluded that a torch position of −4 mm (sampling more upstream in the ICP), seems to be the most suitable for drastically reducing the contribution from $ArAr^+$ to the Se^+ signals, with signal intensities of 0.27 V for $^{80}ArAr^+$ and of 5.47 V for $^{80}Se^+$. It is important to mention that the tuning parameters were shown to be very robust, with signal intensities for Se-ions and Ar-based interferences being consistent across multiple days. Only minor adjustments to the torch position (always within the predefined range) were occasionally necessary.

Although the $ArAr^+$ signal intensity has been drastically reduced under these conditions, the signal for $ArArH^+$ remains relatively high (2.48 V), compromising the accuracy of the signal obtained for the $^{77}Se^+$ signal if not properly accounted for. According to the literature, introducing CH_4 into the plasma has proven effective in reducing the occurrence of $ArAr^+$ and, more notably, $ArArH^+$ while also enhancing the Se signal by a factor of 1.5 due to the carbon effect.[22,26,31,32] Therefore, to further suppress the contribution from $ArArH^+$ under the optimized conditions, the impact of CH_4 addition was assessed, as discussed in the following section.

3.2. Effect of methane addition

Methane gas (2% CH_4 in Ar) was introduced into the ICP *via* the additional gas port of the HG unit (Fig. S1†). Various flow rates were tested to evaluate their impact on the signal intensities for the Se^+ and Ar-based ions under the previously optimized plasma conditions. The results obtained are presented in Fig. 2.

Under the optimized conditions (carrier gas 1.2 L min^{-1}, sampling depth of −4 mm and y and x positions of −0.6 mm and 2.33 mm), increasing the CH_4 flow rate led to a nearly 2-fold decrease in the signal intensities for both Se and Ar-based interfering ions upon addition of 1 mL min^{-1} of CH_4 gas only. Consequently, no further CH_4 flow rate testing was performed under these conditions. When the carrier gas flow rate was slightly reduced to 1.1 L min^{-1} (Fig. 2(b)), a similar trend of signal suppression was observed. However, at 1.0 L min^{-1} (Fig. 2(c)), a different trend was observed. The Se signal intensity increased by a factor of 2 when the CH_4 flow rate was increased to approximately 0.8–1.0 mL min^{-1}, while the $ArAr^+$ signal intensity decreased by a similar factor. This behavior aligns with the observation previously reported in the literature.[26] Surprisingly, the $ArArH^+$ signal intensity increased with the addition of CH_4, reaching a maximum of 0.9 V at a flow rate of 1.0 mL min^{-1}. This result contrasts with findings in the literature, where CH_4 addition is reported to significantly decrease the $ArArH^+$ intensity. This discrepancy is likely due to differences in the plasma

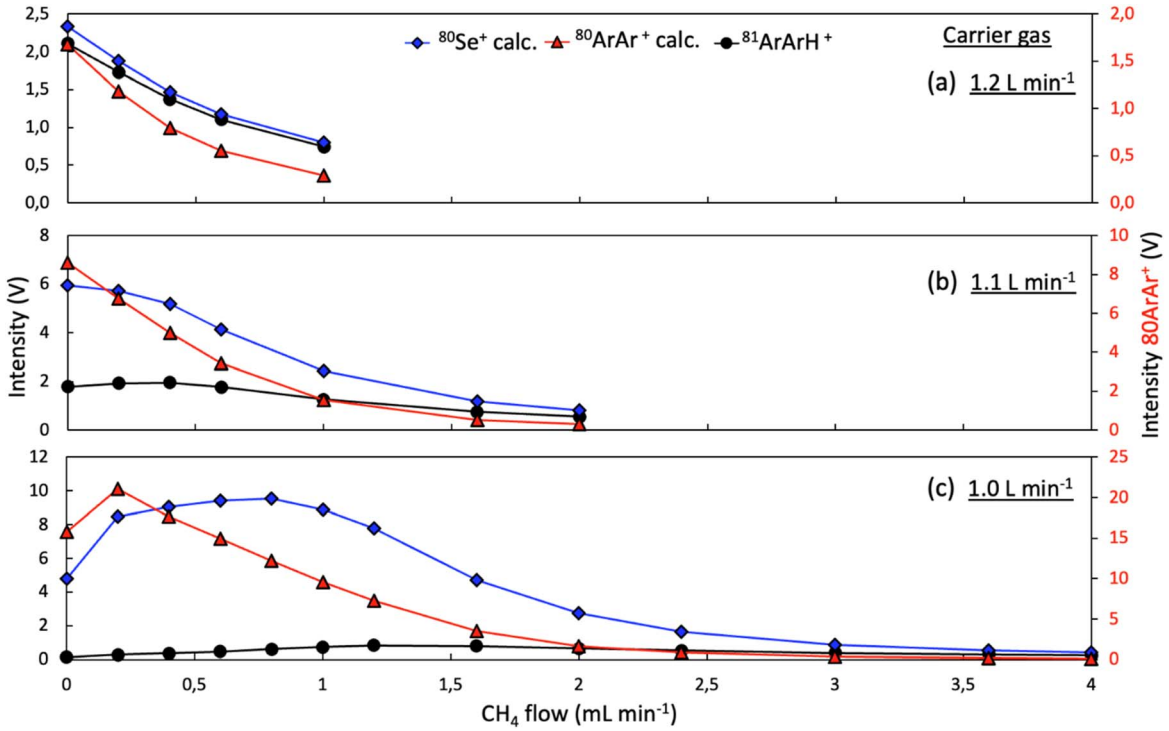

Fig. 2 Effect of CH_4 addition on $^{80}Se^+$, $^{80}ArAr^+$ and $^{81}ArArH^+$ signal intensities, at different carrier gas flow rates.

parameters used in our study as compared to those in previously reported work. Despite this increase, the $ArArH^+$ intensity remains approximately 2.5-fold lower than that observed under our optimized conditions without CH_4 addition (Section 3.1). Beyond 1.0 mL min^{-1} of CH_4, the signal intensities for both Se^+ and the Ar-based interfering ions begin to decline, mirroring the trend observed in Fig. 2(a) and (b). In addition, the signal intensities for $ArAr^+$ and $ArArH^+$ observed when introducing a 2 M HCl blank solution were compared under optimized conditions (i) without CH_4 addition (Fig. 3(a)) and (ii) with CH_4 addition (Fig. 3(b)).

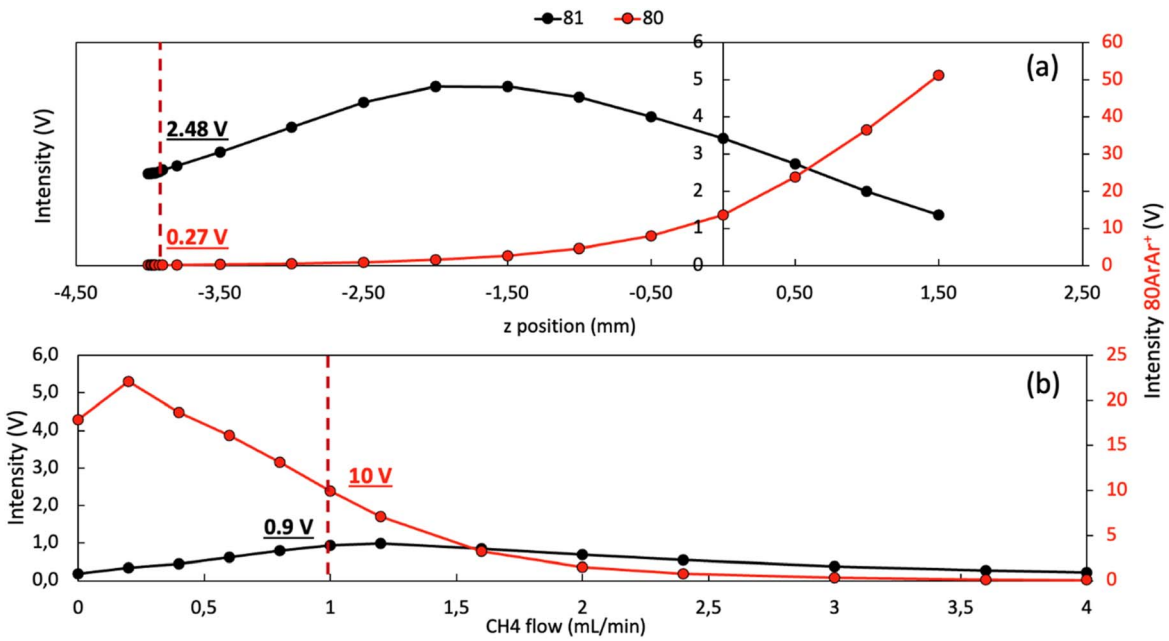

Fig. 3 Comparison of the signal intensities for $ArAr^+$ and $ArArH^+$ (a) without CH_4 addition, under optimized plasma conditions and (b) with CH_4 addition.

The results show that optimizing the plasma settings and sampling at higher sampling depth significantly reduces the contribution from $ArAr^+$ to the signal monitored, with only 0.27 V observed at m/z 80 for the blank. However, although CH_4 addition does reduce the intensity of the signal at mass 80 as reported in the literature, the remaining contribution from the blank under optimized conditions (signal intensity of 10 V) remains relatively high – approximately 40-fold higher than the value obtained without CH_4 addition. In contrast, the $ArArH^+$ signal is significantly lower (about 3-fold lower) when CH_4 is added to the plasma, compared to the conditions without CH_4. Based on these observations, we prioritized the substantial reduction in the contribution from $ArAr^+$ achieved by optimizing the instrument settings without the addition of CH_4, as $ArAr^+$ represents a major interferent affecting two of the Se isotopes, ^{76}Se and ^{78}Se. Consequently, these optimized conditions were selected for all subsequent analyses. Given the relatively high contribution from $ArArH^+$ observed under these conditions, we focused on $\delta^{82/78}Se$ and $\delta^{82/76}Se$ and omitted $\delta^{82/77}Se$ due to the potentially high contribution from $ArArH^+$ at an $m/z = 77$. The contribution was too prominent for accurate correction using the OPZ correction only.

3.3. Effect of sampling depth on measurement accuracy and precision

After evaluating the effect of the instrument settings on the signal intensities of Se and interfering ions, their impact on the accuracy and precision of Se isotope ratio measurements was assessed. Therefore, three different z positions (sampling depths) were selected (Fig. S2†): (i) a sampling depth of 1.5 mm (position far from the sampler cone, sampling more downstream in the plasma), which showed a maximum contribution from $ArAr^+$ to the signal at $m/z = 80$ (Fig. 1(c)), (ii) a sampling depth of 0 mm, at which nearly equal contributions from Se^+ and $ArAr^+$ were observed and finally, (iii) a sampling depth of −4 mm (position very close to the sampling cone, sampling more upstream in the plasma), which showed a dominant contribution of $^{80}Se^+$ to the signal at $m/z = 80$.

In order to evaluate the impact of the sampling depth on the accuracy of Se isotope ratio measurements, a Se Merck solution (LOT HC44697996), previously characterized for its Se isotopic composition,[22] was measured at the three above-mentioned sampling depths and at three concentrations (25, 50, and 100 μg L^{-1}). The bias introduced by instrumental mass discrimination was corrected for using external correction with a standard measured in a SSB approach following the application of the OPZ and hydride corrections described in the Experimental section. The final results for $\delta^{82/78}Se$ and $\delta^{82/76}Se$ are shown in Fig. 4.

At 1.5 mm sampling depth, the accuracy and precision of the Se isotope ratio measurement is compromised, especially at the lowest concentration levels of 25 μg L^{-1}, with $-0.48 \pm 0.28‰$ and $+0.98 \pm 2.37‰$ for $\delta^{82/78}Se$ and $\delta^{82/76}Se$, respectively (reference value -0.72 ± 0.07 and -1.07 ± 0.16, as reported by Chang *et al.* 2017 [22]). This can be explained by the low signal intensity for the Se isotopes monitored at such a low concentration (0.689 V for ^{82}Se) and therefore, the high contribution of the interference to the signal intensity (1.1% contribution from $^{78}ArAr^+$ at $m/z = 78$ and 13% contribution from $^{76}ArAr^+$ at $m/z = 78$, see the ESI†). Such a contribution is too significant to be accurately accounted for using the OPZ correction. At 0 mm sampling depth, with nearly equal contributions from the Se^+ and interference signals, the values were accurate and precise for $\delta^{82/78}Se$ with $-0.72 \pm 0.13‰$ and $-0.69 \pm 0.06‰$ at 50 and 100 μg L^{-1}, respectively (less than 0.5% contribution from $^{78}ArAr^+$), except at 25 μg L^{-1} where $\delta^{82/78}Se$ showed high 2SD values $-0.78 \pm 0.32‰$ (0.8%

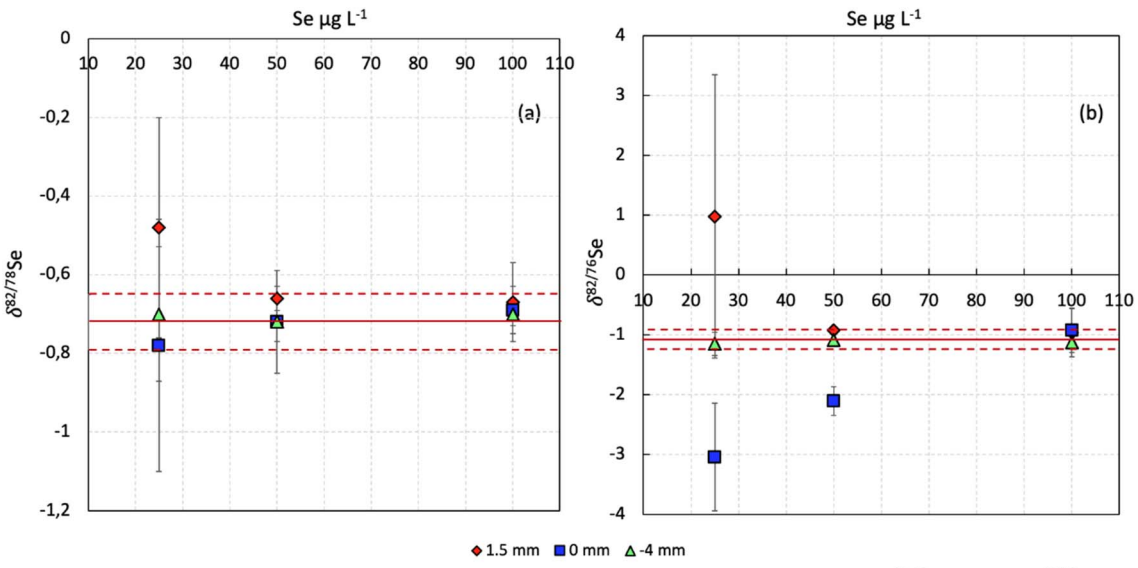

Fig. 4 Effect of the sampling depth (z position of the torch) on the accuracy and precision of $\delta^{82/78}Se$ (a) and $\delta^{82/76}Se$ (b) at 25, 50 and 100 μg L^{-1} of Se. The full red line represents the value of the Se Merck solution obtained by Chang *et al.*[22] and the dotted red lines represent the corresponding ±2SD range. The dots represent the mean value of $n \geq 3$ measurements and the error bars represent the 2SD.

contribution from $^{78}ArAr^{+}$). In contrast, the values are inaccurate and imprecise for $\delta^{82/76}Se$, with $-3.04 \pm 0.90‰$, $-2.10 \pm 0.24‰$ and -0.92 ± 0.37 for 25, 50 and 100 μg L^{-1} of Se, respectively, due to the significant contribution from $ArAr^{+}$ at $m/z = 76$ (2.7–9% contribution). Finally, at −4 mm sampling depth, the values are accurate and precise for both ratios (*e.g.*, $-0.72 \pm 0.05‰$ and $-1.08 \pm 0.04‰$ for $\delta^{82/78}Se$ and $\delta^{82/76}Se$, respectively, at 50 μg L^{-1} of Se), except at 25 μg L^{-1} for which the precision was degraded (ex. $-0.70 \pm 0.17‰$ and $-1.15 \pm 0.38‰$ for $\delta^{82/78}Se$ and $\delta^{82/76}Se$, respectively) due to the low signal intensity obtained for the Se^{+} signals (0.157 V for ^{76}Se, 0.4105 V for ^{78}Se and 0.1637 V for ^{82}Se). At this position, the contribution from $^{78}ArAr^{+}$ to the signal at $m/z = 78$ ranged between 0.03% and 0.1%, only, and the contribution from $^{76}ArAr^{+}$ to the signal at $m/z = 76$ ranged between 0.4 and 1.4% at 100 and 25 μg L^{-1} of Se, respectively. These values highlight the effective reduction of Ar-based interferences under the plasma conditions selected, resulting in improved accuracy and precision of the Se isotope ratio measurements.

3.4. Effect of standard/sample concentration mismatch

To ensure an accurate correction of instrumental mass discrimination using external calibration with a standard measured by the SSB approach, it is crucial to closely match the elemental concentration of the samples and the bracketing standard. To determine the tolerable range of concentration mismatch under the conditions selected, the NIST SRM 3149 bracketing standard was maintained at 50 μg L^{-1}, while the Se Merck solution was prepared with concentrations deviating from −25% to +30% compared to that of the standard. The results obtained under these conditions are presented in Fig. 5.

The values obtained for $\delta^{82/78}Se$ and $\delta^{82/76}Se$ are accurate, even at −25% and +30% concentration mismatch between the sample and the bracketing standard. It is important to emphasize that while the amplitude of the mass bias is influenced by the analyte concentration and matrix composition, it is also systematically influenced by instrumental conditions.[33] Andrén *et al.* (2004) showed that the torch position (sampling depth) has a significant impact on the magnitude and stability of the mass bias. They reported that when the torch is moved closer to the sampler cone, the intensity of the ion beam dropped by almost 20% and the amplitude of the mass bias increased; however, the mass bias was more stable and the precision of the isotope ratio measurement was improved.[33] These findings may help explain the results presented in Fig. 5, where the mass bias appears largely unaffected by concentration mismatch. This could be attributed to the stable operating conditions and the stable mass bias achieved at a torch position of −4 mm, as similarly reported by Andrén *et al.* (2004). Despite this wide tolerable range of sample-standard mismatch, a maximum of 10% mismatch was adopted throughout the remainder of this study as this is the standard range used for most isotope systems in our laboratory.

3.5. Effect of As

Arsenic, potentially present in the sample, readily reacts with $NaBH_4$ in the HG unit by forming $^{75}AsH_3$ and further reaches the MC-ICP-MS unit where next to $^{75}As^{+}$, also $^{75}AsH^{+}$ is formed, causing spectral interference affecting $^{76}Se^{+}$. Isolation of Se using TCP largely removes As. However, some traces might still remain (*e.g.*, for shale rocks, the average As/Se before isolation is 13.5 and rarely exceeds 0.3 after isolation, but for some shales with an exceptionally high original As/Se ratio, the ratio post TCP chemistry might exceed this[29]). The spectral overlap caused by the remaining As can be corrected for mathematically, as shown in Section 2.4 of the Experimental part. However, if the occurrence of As is significant, the correction might no longer be accurate. In this section, the effect of residual As on the accuracy of Se isotope ratio measurements and the reliability of the mathematical correction were evaluated by spiking the Se Merck solution with As at As/Se ratios varying between 0 and 0.5. The results obtained for $\delta^{82/78}Se$ and for $\delta^{82/76}Se$ following mathematical corrections at $m/z = 76$ (see Section 2.4) are shown in Fig. 6.

The $\delta^{82/78}Se$ values remain accurate regardless of the As/Se ratios, since ^{78}Se is not affected by spectral interferences from this element. In contrast, $\delta^{82/76}Se$ is significantly impacted, even

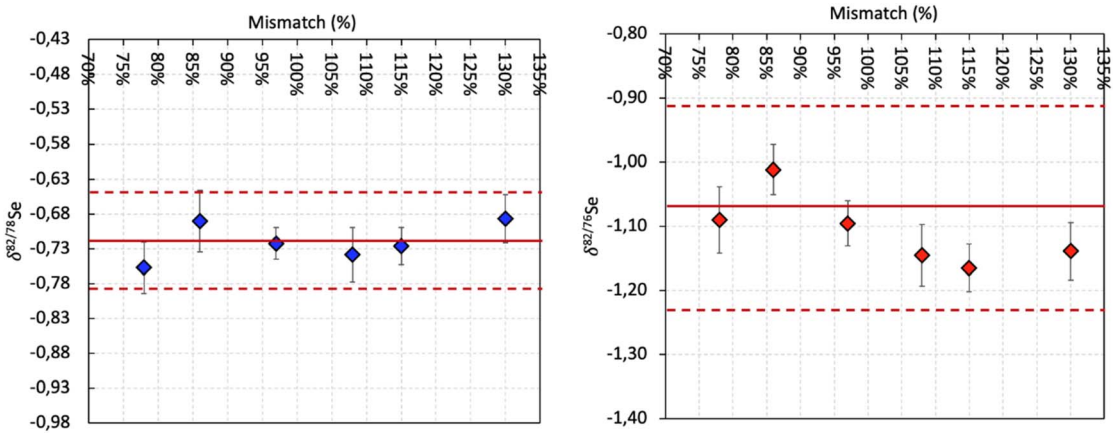

Fig. 5 Effect of sample-standard concentration mismatch on the accuracy of $\delta^{82/78}Se$ and $\delta^{82/76}Se$. The diamond-shaped dots represent the value obtained for a single measurement and the error bars represent the 2SE (internal error).

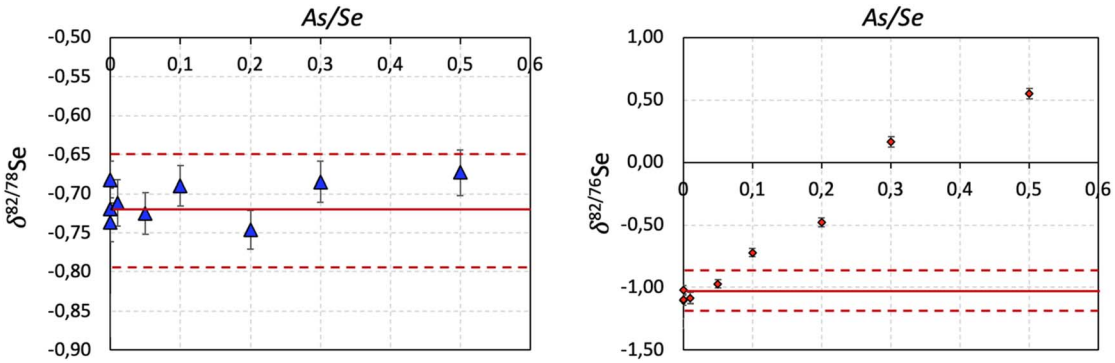

Fig. 6 Effect of different As/Se ratios on the accuracy of $\delta^{82/78}$Se and $\delta^{82/76}$Se values. For $\delta^{82/76}$Se, the values presented are obtained after applying mathematical correction at $m/z = 76$. The dots represent the value obtained for a single measurement and the error bars represent the 2SE (internal error).

at As/Se ratios as low as 0.1. As mentioned previously, significant spectral interference affecting the monitoring of ^{76}Se is caused by the formation of $^{75}AsH^+$. Under the conditions used, this interference can be reliably corrected for up to an As/Se ratio of 0.05, yielding a $\delta^{82/76}$Se value of −0.97‰ (compared to −1.87‰ without correction). However, at higher ratios, the correction is no longer fit-for-purpose. For example, for an As/Se ratio of 0.1, the uncorrected value of −2.55‰ is adjusted to −0.72‰ after correction. This trend of over-correction continues with increasing As/Se ratios, resulting in increasingly heavier values – for example, at a ratio of 0.5, the corrected $\delta^{82/76}$Se shifts to +0.55‰, whereas the uncorrected value is at −8‰. This contrasts with the results reported in the literature, where As/Se ratios up to 0.6 were reliably corrected for using the same mathematical correction, combined with a double-spike correction approach.[23,29] This inconsistency with the results reported in the literature can be explained by the high hydride formation rate of $\sim 7 \times 10^{-3}$ (calculated for $^{82}SeH^+/^{82}Se^+$ according to eqn (7)) obtained under our experimental conditions, which is higher than the values reported in the literature ($\sim 10^{-3}$–10^{-4}).[29] When it is assumed that the AsH^+/As^+ ratio is identical to $^{82}SeH^+/^{82}Se^+$ (eqn (10)), the AsH^+ formation under the conditions used is significant even at low As/Se ratios. This constitutes a limitation for the method, making it only suitable for samples showing an As/Se content ≤0.05 post TCP chemistry, or for samples without As. For samples with high As concentrations, a further optimization of the TCP separation conditions will be necessary to achieve lower residual As/Se ratios.

3.6. Long-term reproducibility

The long-term reproducibility of the $\delta^{82/78}$Se values obtained with this method was assessed by tracking the values obtained for Se Merck solution ($N = 120$), measured over a period of 18 months (August 2023–January 2025). The results obtained for 2 concentration levels 100 and 50 μg L^{-1} are summarized in Fig. 7.

The average of all $\delta^{82/78}$Se values obtained for the Se Merck solution is −0.71 ± 0.07 (2SD, $n = 120$), in accordance with the values previously reported by Chang *et al.*[22] for the same solution (reference value −0.72 ± 0.07). This further demonstrates the method's robustness and suitability for accurate and precise Se isotope ratio measurements.

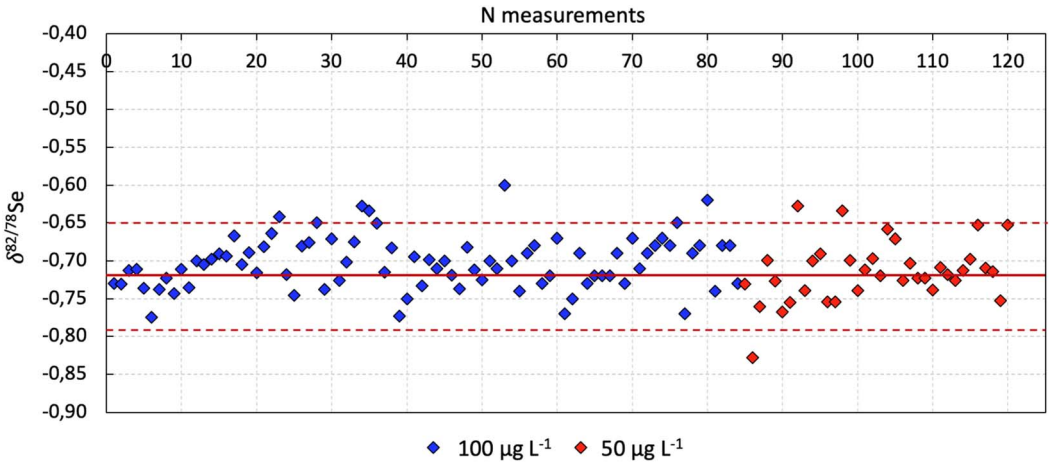

Fig. 7 $\delta^{82/78}$Se values ($n = 120$) obtained over an 18 month period at 50 and 100 μg L^{-1} of Se.

Table 3 X/Se ratio before and after isolation of the samples using the TCP method; Se recovery (%) from the column (mean ± SD, $n = 3$)

		Fe/Se	Co/Se	Ni/Se	Cu/Se	As/Se	Se recovery (%)
Liver	**Before isolation**	**5.78**	**0.01**	**0.04**	**5.07**	**0.29**	101 ± 3%
	After isolation	0.05	0.00	0.00	0.01	0.05	
Spleen	**Before isolation**	**18.25**	**0.00**	**0.00**	**0.01**	**0.02**	97 ± 3%
	After isolation	0.02	0.00	0.00	0.00	0.01	
Kidney	**Before isolation**	**18.26**	**0.01**	**0.01**	**3.08**	**0.12**	96 ± 2%
	After isolation	0.03	0.00	0.00	0.01	0.02	
Intestine	**Before isolation**	**4.90**	**0.00**	**0.02**	**0.42**	**0.57**	98 ± 3%
	After isolation	0.16	0.00	0.02	0.02	0.08	

3.7. Validation and application to tuna fish organs

For validating the proposed method, the Se-enriched yeast (SELM-1) reference material, previously characterized for its Se isotopic composition by other groups, has been digested, and subjected to TCP for isolating Se from the matrix, and subsequently to MC-ICP-MS measurement under the optimized conditions. Se was quantitatively recovered upon TCP purification, thus avoiding any impact of potential fractionation effects on the final results. The Se isotopic composition measured for SELM-1 was −0.77 ± 0.11‰ ($n = 3$, 2SD) for $\delta^{82/78}$Se, and −1.16 ± 0.42‰ ($n = 3$, 2SD) for $\delta^{82/76}$Se, which is in agreement with the values reported in the literature (−0.66 ± 0.29‰,[34] −0.68 ± 0.02‰,[35] −0.70 ± 0.07‰ [36] and −0.69 ± 0.06‰ [37] for $\delta^{82/78}$Se and −0.97 ± 0.3‰ [34] for $\delta^{82/76}$Se), thus validating the method.

Finally, the validated method was applied to a set of tuna fish organs (liver, spleen, kidney, and intestine), previously characterized for their Hg concentration, speciation and isotopic composition. The aim of this kind of work is to study the role of Se in the Hg detoxification process through monitoring its concentration and isotopic composition. The different fish organs have been subjected to acid digestion and to Se isolation using the TCP method in triplicate. The Se recovery (%) and information on the elemental composition of these samples before and after isolation (represented as the X/Se ratio, with X being the element of interest) are summarized in Table 3.

For all organs analyzed in triplicate, Se was quantitatively eluted from the column, with recovery factors ≥96% ± 2%. Moreover, critical elements known to interfere with the hydride generation process (Fe, Co, Ni, and Cu) and those causing spectral interference affecting the signals of the Se isotopes of interest (As), were efficiently removed from the matrix, with an X/Se ratio post TCP chemistry of $0 \leq X/Se \leq 0.16$. The As/Se ratio in the sample prior to TCP was already low (≤0.57) and was further reduced following the TCP purification, now ranging between 0.01 and 0.05 (except for the intestine for which it was slightly higher). These residual As/Se ratios fall within the acceptable range for accurate mathematical correction, as previously demonstrated in Section 3.5.

Subsequently, the purified Se fractions were subjected to MC-ICP-MS measurement using the previously developed method at a Se concentration of 100 μg L^{-1}. Throughout the sequence, the Se Merck solution was measured as a quality control solution at the beginning and at the end of the sequence and in-between every 6 samples for monitoring the accuracy of the isotope ratio measurements ($\delta^{82/78}$Se = −0.70 ± 0.09‰ and $\delta^{82/76}$Se = −1.07 ± 0.14‰, Mean ± 2SD, $n = 7$). Furthermore, the $\delta^{82/78}$Se value, obtained for the samples and the Se Merck solution, was plotted as a function of the corresponding $\delta^{82/76}$Se values. The three-isotope plot obtained is provided as Fig. 8.

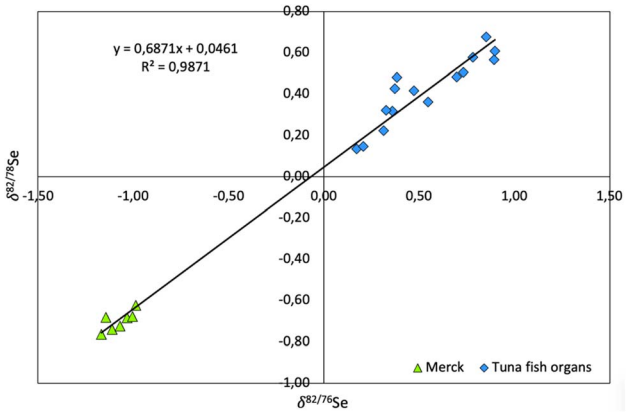

Fig. 8 Three-isotope plot of $\delta^{82/78}$Se *vs.* $\delta^{82/76}$Se of all data points for the tuna fish organs and for the different measurements of the Se Merck solution throughout the sequence.

The $\delta^{82/78}$Se *vs.* $\delta^{82/76}$Se three-isotope plot of Fig. 8 shows a linear trend ($R^2 = 0.9871$), with a slope of 0.6871, which closely matches the slope of the theoretical mass-dependent

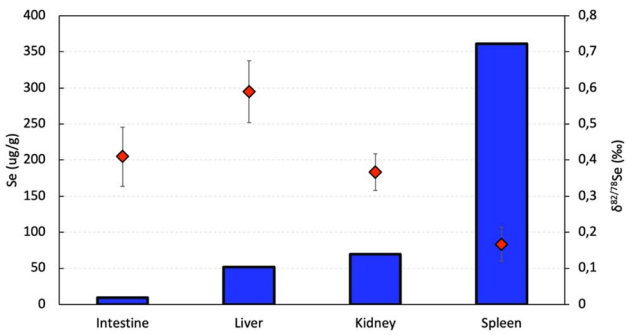

Fig. 9 Se concentration (μg g^{-1}) and isotopic composition ($\delta^{82/78}$Se ‰) measured in the intestine, liver, kidney and spleen of tuna fish. The $\delta^{82/78}$Se values (red diamonds) represent the average value of three replicate analyses (sample preparation included) of the same sample and the error bars represent the 1SD.

fractionation of 0.6497, calculated according to Young *et al.* (2002), assuming thermodynamically governed fractionation.[38] This confirms that our results are accurate and not affected by spectral interference. For a further interpretation of the Se isotopic composition in tuna fish organs, the $\delta^{82/78}$Se results were plotted together with the Se concentration found in each organ. The results are shown in Fig. 9.

As shown in Fig. 9, $\delta^{82/78}$Se values for all tuna fish organs display a Se isotopic composition that is heavier than that of the standard (positive $\delta^{82/78}$Se values). The spleen had the highest Se content and displayed the lightest Se isotopic composition +0.17 ± 0.05‰ (n = 3, 1SD), whereas the liver showed the heaviest $\delta^{82/78}$Se value of all organs measured: +0.57 ± 0.07‰ (n = 6, 1SD). This is consistent with the previous observations of Marchán-Moreno *et al.* (2024)[37] and Clark & Johnson *et al.* (2010)[39] who also reported that the liver of fish (catfish, sunfish and carp) and seabirds (giant petrels) exhibited the heaviest Se isotopic composition of all organs analysed. This was attributed to the liver being the primary site for Se intake from the diet, from which Se is redistributed to other organs for various metabolic functions. The unutilized Se tends to accumulate in the liver and becomes enriched in heavier isotopes, as lighter isotopes are preferentially involved in the metabolic processes.[37] The depletion in the heavier Se isotopes in the other organs (lighter isotopic composition) shown in Fig. 9 supports the hypothesis of lighter Se isotopes being more efficiently distributed from the liver to the other tissues.

When comparing the Se isotopic composition obtained in this work with that of Hg measured in the same organs by Wiech *et al.* (2024),[6] a similar trend is observed. The authors showed that the liver exhibited the heaviest Hg isotopic composition, followed by the intestine and the kidney, while the spleen showed the lightest δ^{202}Hg values. This pattern was attributed to differences in Hg speciation, particularly the methylmercury (MeHg) content, which was the highest in the liver and lowest in the spleen. Since during methylation, there is a slight preference for the heavier Hg isotopes being incorporated, MeHg is enriched in the heavier isotopes compared to inorganic Hg (iHg). Moreover, Wiech *et al.* (2024)[6] reported that the masses of both Hg and Se present in the particulate form were the highest in the spleen and kidney, suggesting that HgSe nanoparticle formation predominantly occurs in these organs. This supports the idea that the spleen and kidney might play a key role in the Hg detoxification process by Se. Although coming from one individual fish only, the Se concentration and isotopic data obtained in this study support this view: in addition to the lowest content of MeHg, the spleen and kidney exhibited the highest Se concentration and the lightest Se isotopic composition. These initial results suggest that isotopic analysis can be an additional tool for investigating whether Se is actively involved in the demethylation of MeHg. It is important to highlight that, to the best of the authors' knowledge, this work is the first reporting data on the Se isotopic composition in marine fish organs and in tuna fish particularly. As such, data interpretation remains tentative due to the very limited availability of Se isotope ratio data in biological systems, particularly in marine organisms. In fact, the only data reported for biological samples are limited to fish and plants from a Se-contaminated lake,[39,40] plankton from the Pacific Ocean,[41] and more recently tissues (liver, kidney, muscle and brain) of a marine top-predator seabird.[37] Therefore, based on these promising initial results, Se isotopic analysis of a wider collection of tuna fish organs (higher number of individuals) can aid in better understanding of the role of Se in Hg detoxification processes in marine fish.

4. Conclusions

In this work, a detailed investigation of the distribution of Se^+ and $ArAr^+/ArArH^+$ ions within the ICP was accomplished through radial and axial spatial profiling. By optimizing the torch position, particularly by sampling the ICP more upstream (sampling depth of −4 mm), Ar-based interferences affecting the Se^+ signals were significantly reduced. Under optimized conditions, the contribution from $^{76}ArAr^+$ and $^{78}ArAr^+$ to the signals at m/z = 76 and = 78 was reduced to 0.4% and 0.03%, respectively, at a Se concentration of 100 μg L^{-1}. This optimization enabled accurate and precise Se isotope ratio measurements, with a 2SD of 0.03‰ and 0.17‰ for $\delta^{82/78}$Se and of 0.08‰ and 0.38‰ for $\delta^{82/76}$Se, at 100 and 25 μg L^{-1}, respectively. These results were obtained after OPZ correction and using external correction for the mass bias with the standard measured in a SSB sequence. Notably, this configuration maintained stable mass bias conditions, delivering accurate data even with up to 30% concentration mismatch between the Se concentration in the sample and bracketing standard. Despite these advantages, the method exhibits some inherent limitations, mainly related to the high hydride formation rate ($\sim 7 \times 10^{-3}$) obtained under the optimized conditions. This resulted in a low tolerance to the presence of residual As in the measured sample solution, as only for As/Se ratios ≤0.05 mathematical correction proved sufficient. Nevertheless, the method demonstrated excellent long-term reproducibility, with a standard deviation of 0.07‰ (2SD) for 120 $\delta^{82/78}$Se measurements across an 18-month period, highlighting its robustness. Finally, the method was validated using the SELM-1 reference material, with values in agreement with those reported in the literature, and was applied, for the first time, to a set of tuna fish organs (spleen, intestine, kidney and liver). These initial results demonstrated organ-specific Se isotopic signatures, indicating the potential of Se isotopic analysis as a powerful tool for tracing metabolic processes of this element and for potentially elucidating its role in Hg detoxification in marine fish.

Data availability

The data supporting this article have been included as part of the ESI.†

Conflicts of interest

There are no conflicts to declare.

Acknowledgements

FWO-Vlaanderen is acknowledged for funding the acquisition of MC-ICP-MS instrumentation (ZW15-02 – G0H6216N). Financial support from Ghent University funding (BOF24J/2021/054) is also acknowledged for providing the grant that enabled the execution of this project. Furthermore, the work was also supported by the Norwegian Ministry of Trade, Industry and Fisheries.

References

1 G. Barchielli, A. Capperucci and D. Tanini, *Antioxidants*, 2022, **11**, 251.
2 M. Roman, P. Jitaru and C. Barbante, *Metallomics*, 2014, **6**, 25–54.
3 M. J. Berry and N. V. C. Ralston, *EcoHealth*, 2008, **5**, 456–459.
4 Z. Gajdosechova, M. M. Lawan, D. S. Urgast, A. Raab, K. G. Scheckel, E. Lombi, P. M. Kopittke, K. Loeschner, E. H. Larsen, G. Woods, A. Brownlow, F. L. Read, J. Feldmann and E. M. Krupp, *Sci. Rep.*, 2016, **6**, 34361.
5 L. Paton, T. T. Moro, T. Lockwood, T. de Andrade Maranhão, G. Gössler, D. Clases and J. Feldmann, *Environ. Sci.: Nano*, 2024, **11**, 1883–1890.
6 M. Wiech, A. M. Bienfait, M. Silva, J. Barre, V. Sele, M. S. Bank, S. Bérail, E. Tessier, D. Amouroux and A. M. Azad, *J. Hazard. Mater.*, 2024, **473**, 134699.
7 A. Manceau, A.-C. Gaillot, P. Glatzel, Y. Cherel and P. Bustamante, *Environ. Sci. Technol.*, 2021, **55**, 1515–1526.
8 J. Brozmanova, D. Manikova, V. Vlčkova and M. Chovanec, *Arch Toxicol.*, 2010, **84**, 919–938.
9 L. H. E. Winkel, C. A. Johnson, M. Lenz, T. Grundl, O. X. Leupin, M. Amini and L. Charlet, *Environ. Sci. Technol.*, 2012, **46**, 571–579.
10 A. Fernandez-Martınez and L. Charlet, *Rev. Environ. Sci. Biotechnol.*, 2009, **8**, 81–110.
11 D. Perrone, M. Monteiro and J. C. Nunes, in *Food and Nutritional Components in Focus*, ed. V. R. Preedy, Royal Society of Chemistry, Cambridge, 2015, pp. 3–15.
12 F. Vanhaecke and K. Kyser, in *Isotopic Analysis*, John Wiley & Sons, Ltd, 2012, pp. 1–29.
13 P. A. E. Pogge von Strandmann, E. E. Stüeken, T. Elliott, S. W. Poulton, C. M. Dehler, D. E. Canfield and D. C. Catling, *Nat. Commun.*, 2015, **6**, 10157.
14 E. E. Stüeken, J. Foriel, R. Buick and S. D. Schoepfer, *Chem. Geol.*, 2015, **410**, 28–39.
15 K. Mitchell, S. Z. Mansoor, P. R. D. Mason, T. M. Johnson and P. Van Cappellen, *Earth Planet. Sci. Lett.*, 2016, **441**, 178–187.
16 M. A. Kipp, E. E. Stüeken, A. Bekker and R. Buick, *Proc. Natl. Acad. Sci. U. S. A.*, 2017, **114**, 875–880.
17 F. Vanhaecke and L. Moens, *Anal. Bioanal. Chem.*, 2004, **378**, 232–240.
18 F. Vanhaecke, L. Balcaen and D. Malinovsky, *J. Anal. At. Spectrom.*, 2009, **24**, 863.
19 R. S. Houk, *Anal. Chem.*, 1986, **58**, 97A–105A.
20 K. Schilling, T. M. Johnson and W. Wilcke, *Soil Sci. Soc. Am. J.*, 2011, **75**, 1354–1364.
21 T. Kurzawa, S. König, J. Labidi, A. Yierpan and R. Schoenberg, *Chem. Geol.*, 2017, **466**, 219–228.
22 Y. Chang, J. Zhang, J.-Q. Qu and Y. Xue, *Chem. Geol.*, 2017, **471**, 65–73.
23 M.-L. Pons, M.-A. Millet, G. N. Nowell, S. Misra and H. M. Williams, *J. Anal. At. Spectrom.*, 2020, **35**, 320–330.
24 N. Elwaer and H. Hintelmann, *J. Anal. At. Spectrom.*, 2008, **23**, 733.
25 W. Guo, S. Hu, Y. Wang, L. Zhang, Z. Hu and J. Zhang, *Microchem. J.*, 2013, **108**, 106–112.
26 G. H. Floor, R. Millot, M. Iglesias and P. Négrel, *J. Mass Spectrom.*, 2011, **46**, 182–188.
27 H. Banning, M. Stelling, S. König, R. Schoenberg and T. Neumann, *PLoS One*, 2018, **13**, e0193826.
28 A. E. Holliday and D. Beauchemin, *Spectrochim. Acta, Part B*, 2004, **59**, 291–311.
29 P. A. E. Pogge von Strandmann, C. D. Coath, D. C. Catling, S. W. Poulton and T. Elliott, *J. Anal. At. Spectrom.*, 2014, **29**, 1648–1659.
30 M. M. Fraser and D. Beauchemin, *Spectrochim. Acta, Part B*, 2001, **56**, 2479–2495.
31 I. Rodushkin, P. Nordlund, E. Engström and D. C. Baxter, *J. Anal. At. Spectrom.*, 2005, **20**, 1250–1255.
32 G. Grindlay, J. Mora, M. De Loos-Vollebregt and F. Vanhaecke, *Spectrochim. Acta, Part B*, 2013, **86**, 42–49.
33 H. Andrén, I. Rodushkin, A. Stenberg, D. Malinovsky and D. C. Baxter, *J. Anal. At. Spectrom.*, 2004, **19**, 1217–1224.
34 J. Far, S. Bérail, H. Preud'homme and R. Lobinski, *J. Anal. At. Spectrom.*, 2010, **25**, 1695.
35 J. Karasiński, A. Tupys, L. Yang, Z. Mester, L. Halicz and E. Bulska, *Anal. Chem.*, 2020, **92**, 16097–16104.
36 J. Karasiński, K. Tetfejer, P. Radziński, A. Tupys, A. Gambin, E. Bulska and L. Halicz, *Anal. Chem.*, 2024, **96**, 3763–3771.
37 C. Marchán-Moreno, P. Louvat, M. Bueno, S. Berail, W. T. Corns, Y. Cherel, P. Bustamante, D. Amouroux and Z. Pedrero, *Environ. Sci. Technol.*, 2024, **58**, 13434–13443.
38 E. D. Young, A. Galy and H. Nagahara, *Geochim. Cosmochim. Acta*, 2002, **66**, 1095–1104.
39 S. K. Clark and T. M. Johnson, *J. Environ. Qual.*, 2010, **39**, 2200–2210.
40 M. J. Herbel, T. M. Johnson, K. K. Tanji, S. Gao and T. D. Bullen, *J. Environ. Qual.*, 2002, **31**, 1146–1156.
41 K. Mitchell, P. R. D. Mason, P. Van Cappellen, T. M. Johnson, B. C. Gill, J. D. Owens, J. Diaz, E. D. Ingall, G.-J. Reichart and T. W. Lyons, *Geochim. Cosmochim. Acta*, 2012, **89**, 302–317.

